

# Monte Carlo study on the low momentum $\mu$ - $\pi$ identification of the BESIII EM calorimeter

WANG Zhi-Gang(王志刚)<sup>1,2,1)</sup> LÜ Jun-Guang(吕军光)<sup>1</sup> HE Kang-Lin(何康林)<sup>1</sup>  
 AN Zheng-Hua(安正华)<sup>1,2</sup> CAI Xiao(蔡啸)<sup>1</sup> DONG Ming-Yi(董明义)<sup>1</sup> FANG Jian(方建)<sup>1</sup>  
 HU Tao(胡涛)<sup>1</sup> LIU Wan-Jin(刘万金)<sup>1</sup> LÜ Qi-Wen(吕绮雯)<sup>2,3</sup> NING Fei-Peng(宁飞鹏)<sup>1,3</sup>  
 SUN Li-Jun(孙丽君)<sup>1</sup> SUN Xi-Lei(孙希磊)<sup>1,2</sup> WANG Xiao-Dong(王晓东)<sup>1,3</sup> XUE Zhen(薛镇)<sup>1,4</sup>  
 YU Bo-Xiang(俞伯祥)<sup>1</sup> ZHANG Ai-Wu(章爱武)<sup>1,2</sup> ZHOU Li(周莉)<sup>1</sup>

<sup>1</sup> (Institute of High Energy Physics, CAS, Beijing 100049, China)

<sup>2</sup> (Graduate University of Chinese Academy of Science, Beijing 100049, China)

<sup>3</sup> (Shanxi University, Taiyuan 030006, China)

<sup>4</sup> (University of Science and Technology of China, Hefei 230026, China)

**Abstract** The BESIII detector has a high-resolution electromagnetic calorimeter which can be used for low momentum  $\mu$ - $\pi$  identification. Based on Monte Carlo simulations,  $\mu$ - $\pi$  separation was studied. A multilayer perceptron neural network making use of the defined variables was used to do the identification and a good  $\mu$ - $\pi$  separation result was obtained.

**Key words** BESIII calorimeter, particle identification, artificial neural network

**PACS** 29.30.Aj

## 1 Introduction

For  $e^+e^-$  collision physics, the measurement of muons is of great importance. In the discovery of  $J/\psi$ , the narrow sharp enhancement of the cross section is one of the most important pieces of evidence. The energy dependence of the  $e^+e^- \rightarrow \mu^+\mu^-$  cross section has proved that the quantum electrodynamics is correct up to  $10^{-16}$  cm. The precise measurement of  $\tau$  mass at BESIII is also carried out mainly by selecting the  $e\mu$  final state events. As for the study of the general problems in  $e^+e^-$  collision physics, since the final states contain muons, this needs fine muon measurement.

For some important physics process, especially for some rare decay channel measurements, the ability of  $\mu$ - $\pi$  identification affects the physical result to a great extent. For instance, the measurement of the purely leptonic decay branching fraction in charm physics, some rare decays in charm and  $\tau$  decays such as  $D^0 \rightarrow \mu^+\mu^-$  rely on the measurement of muons. In the upcoming BESIII experiment there will be a large

number of muons produced in  $D$  and  $\tau$  decays.

Since the masses of muons and pions are so close, they cannot be identified by the Time Of Flight (TOF) and ionization energy loss ( $dE/dX$ ) information. Usually muons are identified by the muon detector, the outermost subsystem of the spectrometer. The cut-off momentum, the lowest momentum of muons the BESIII muon detector<sup>[1]</sup> (MUC) can identify, is about 400 MeV/ $c$ . Since there is a 1 T magnetic field, the trajectory of the charged particle will bend along with its momentum; if the momentum of a muon is lower than 400 MeV/ $c$ , the muon will lose most of its energy before it hits in the MUC, so it cannot be detected by the MUC. The discrimination of  $\mu$ - $\pi$  below 400 MeV/ $c$  is a vacancy in the BESIII PID<sup>[2]</sup> at present. The transverse momentum distributions of muons produced in  $\tau$  and  $D$  decays at  $E_{cm} = 4.0$  GeV are shown in Fig. 1. It can be seen that muons produced at the energy relevant to us are mostly beyond the range that can be identified by MUC, so the study of low momentum  $\mu$ - $\pi$  identification is of great significance.

Received 26 December 2008, Revised 23 February 2009

1) E-mail: wangzhg@ihep.ac.cn

©2009 Chinese Physical Society and the Institute of High Energy Physics of the Chinese Academy of Sciences and the Institute of Modern Physics of the Chinese Academy of Sciences and IOP Publishing Ltd

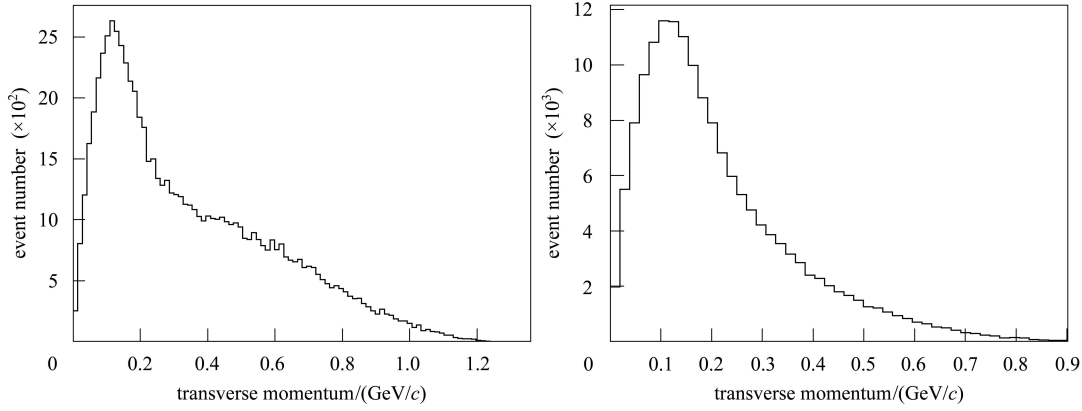


Fig. 1. The transverse momentum distributions of muons produced in  $\tau$  and D decays at  $\sqrt{s}=4.0$  GeV.

## 2 Beam test

The  $dE/dX$  energy resolution of the calorimeter was tested using proton and pion beams at the E3<sup>[3]</sup> beam line of IHEP, with a momentum of 700 MeV/ $c$ . An array of  $6 \times 4$  CsI(Tl) crystals with the same mechanical assembly and readout electronics as those of the BESIII calorimeter were used. The crystal configuration of the beam test is illustrated in Fig. 2. The test beams were incident on the center of the side face of the 2nd layer crystals, with the beam direction perpendicular to the side face of the crystals. In the BESIII experiment the low momentum charged particle will pass the side face of crystal under the magnetic field, so we used the beam test to simulate the BESIII experiment. The deposited energy distributions of pions and protons in the 6 crystals of the 2nd layer are shown in Fig.3. As can be seen in Fig. 3, the pion will pass all of the six crystals and the deposited energies have similar distributions, while the proton will pass only three crystals and the deposited energy distributions have quite different shapes. The  $dE/dX$  resolution of a single crystal obtained by

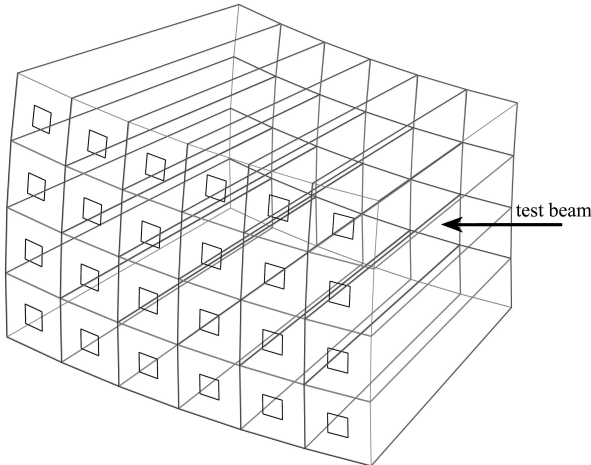


Fig. 2. The experimental configuration of beam test.

fitting the experimental data can be achieved to 6% for 700 MeV/ $c$  pion. In view of the good  $dE/dX$  resolution of the calorimeter, low momentum  $\mu$ - $\pi$  identification by the calorimeter was studied.

## 3 Event samples

In order to study the behaviour of low momentum muons and pions in the calorimeter, the single particle simulation<sup>[4]</sup> and reconstruction were done under the BES Offline Software System<sup>[5]</sup> (BOSS). Single muon and pion events with the momentum ranging from 200 MeV/ $c$  to 400 MeV/ $c$  with step of 50 MeV/ $c$  were simulated and reconstructed respectively.

## 4 Discriminating variables

Muons and pions can be separated by analysis of their deposited energy distributions in the calorimeter. In this analysis, the deposited energy and the hit crystals were calculated only within the reconstructed cluster<sup>[6]</sup>. After studying and comparing the simulation data in detail, several discriminating variables were defined. In Fig. 4 to Fig. 10 the angle  $\theta$  (the polar angle in the BESIII  $e^+e^-$  collision experiment) of the incident muons or pions is  $90^\circ$ .

### (1) Total energy deposited in the calorimeter

The energy of muons deposited in the calorimeter is mainly by ionization, while a fraction of pions will have nuclear interaction with the crystals. So the total deposited energy distribution of pions is wider than that of muons, as shown as Fig. 4. There are two peaks in the total deposited energy distribution of muons when the momentum is around 350 MeV/ $c$ , because a fraction of muons will pass through the crystal by ionization while a fraction of muons will lose all energy and stop in the crystal. This will lead to a potential for particle misidentification.

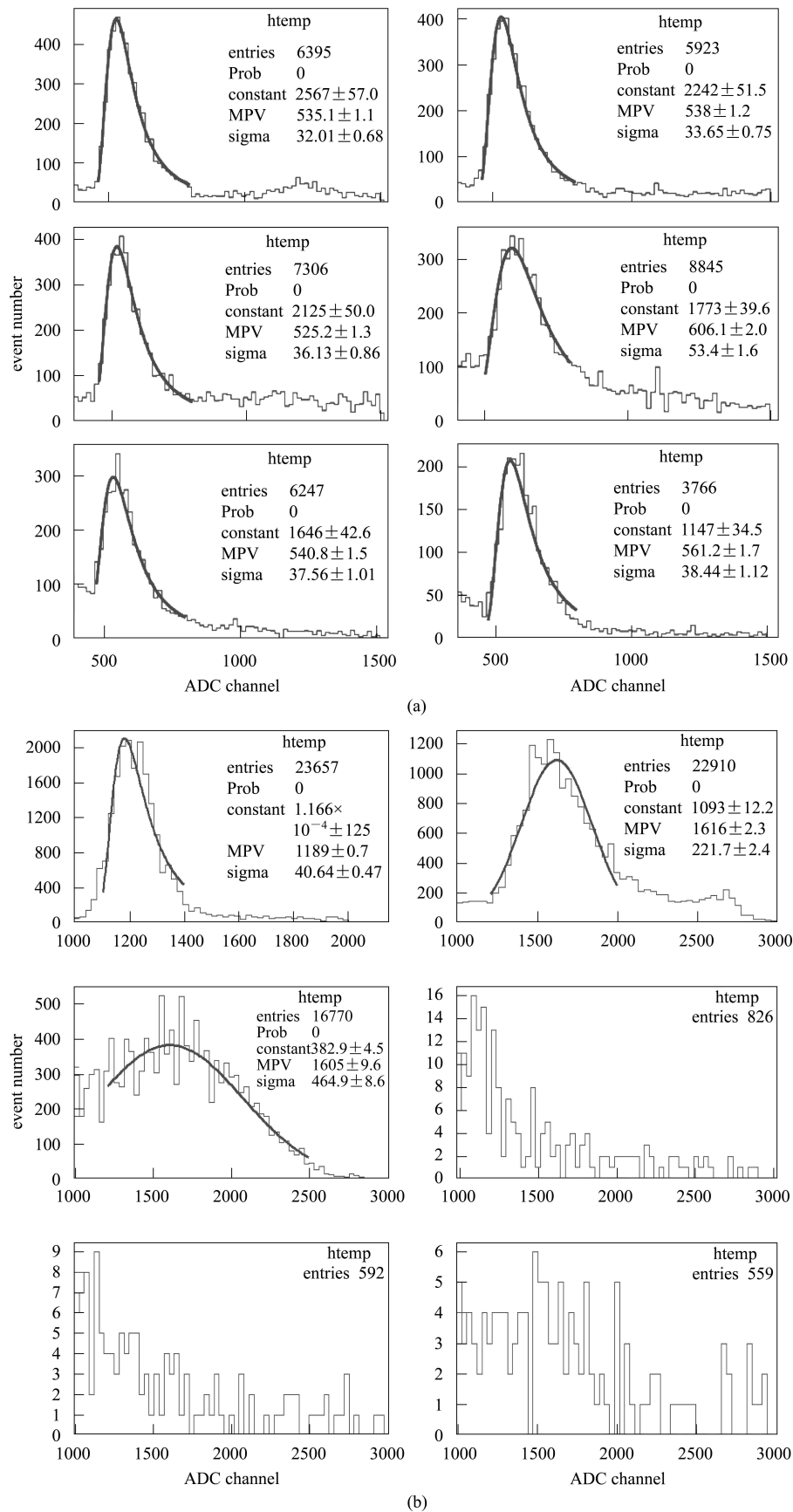


Fig. 3. The deposited energy distributions of pions and protons in 6 crystals. (a) Deposited energy distribution of pions (ADC); (b) deposited energy distribution of protons (ADC).

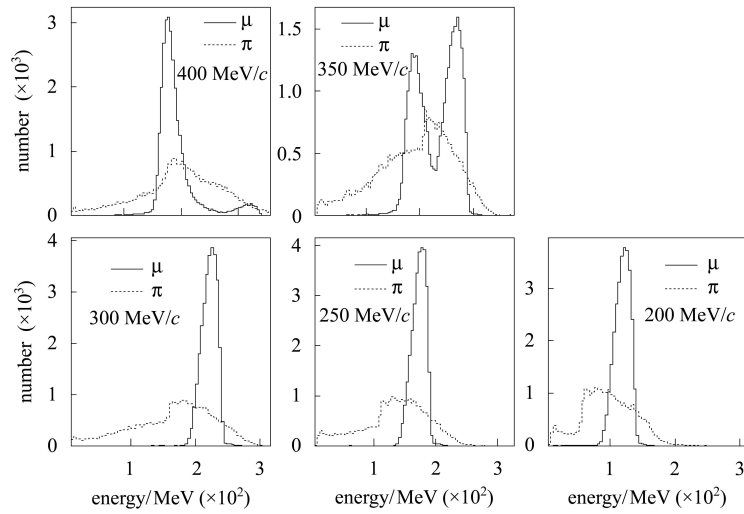


Fig. 4. Total energy deposited in the calorimeter for different momenta. Solid line stands for muons and dashed line stands for pions.

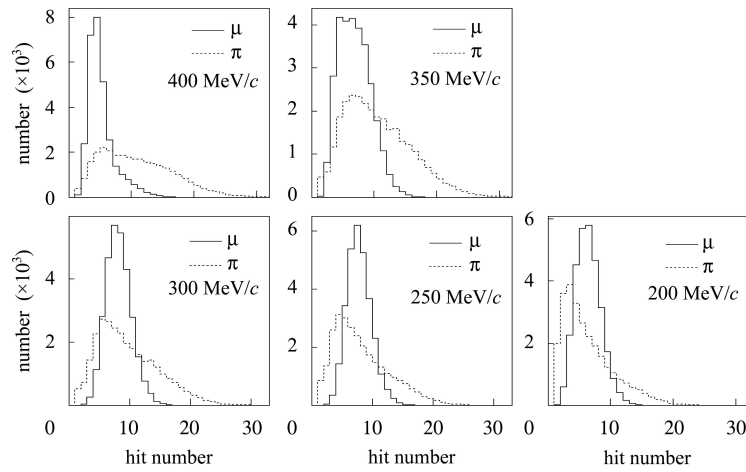


Fig. 5. Hit number of crystals in the calorimeter for different momenta. Solid line stands for muons and dashed line stands for pions.

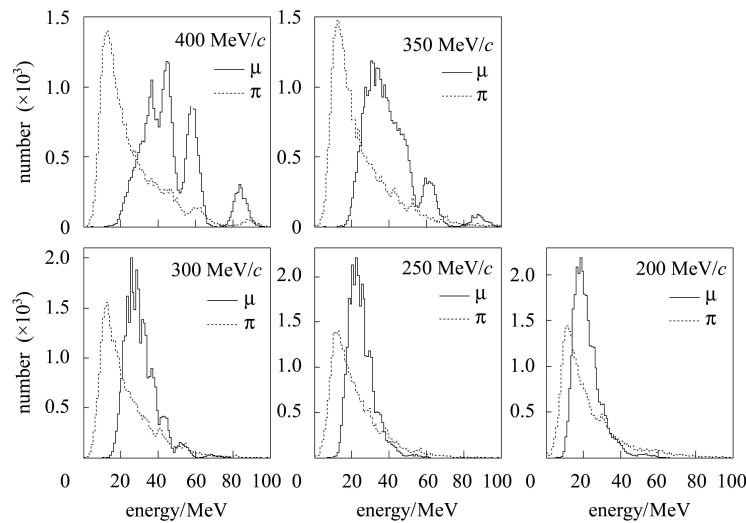


Fig. 6. Average energy deposited in the calorimeter for different momenta. Solid line stands for muons and dashed line stands for pions.

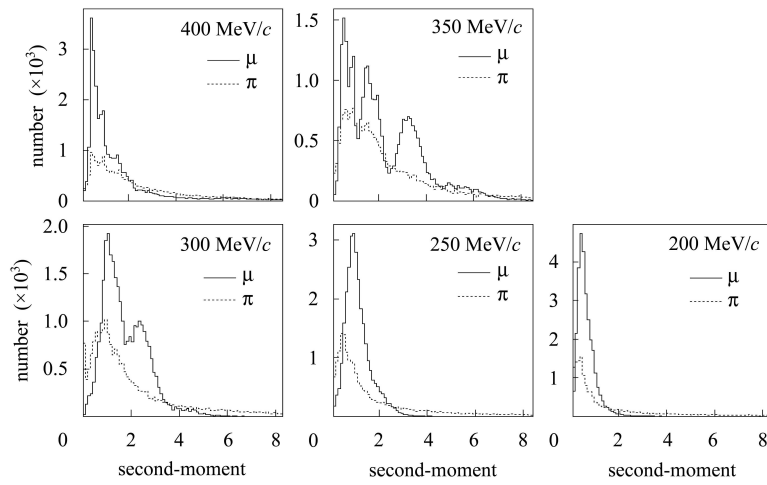


Fig. 7. Second-moment  $S$  for different momenta. Solid line stands for muons and dashed line stands for pions.

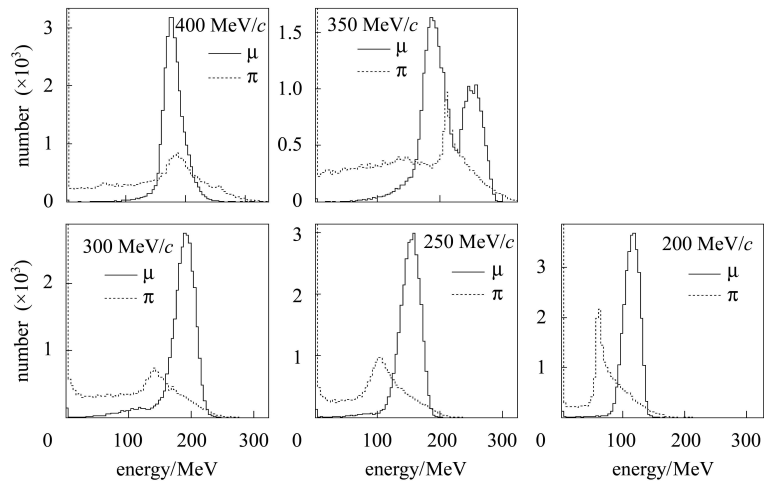


Fig. 8. Energy deposited along the extrapolated path for different momenta. Solid line stands for muons and dashed line stands for pions.

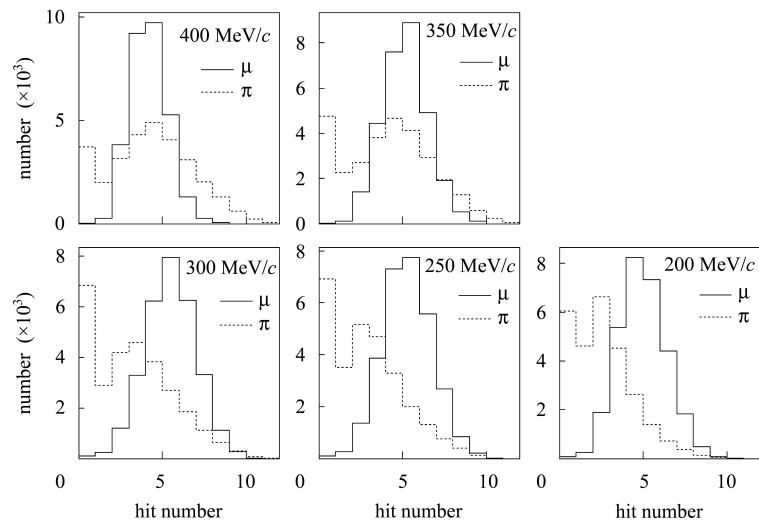


Fig. 9. Number of crystals along the extrapolated path for different momenta. Solid line stands for muons and dashed line stands for pions.

## (2) Number of hit crystals in the calorimeter

In this analysis, all the hit crystals in the reconstructed cluster were counted. Since pions will have nuclear interaction with the crystals, the energy distribution is wider than muons, and the hit number of pions is larger than that of muons.

## (3) Average energy deposited in each hit crystal

Since the deposited energy of muons is focused on several crystals, the distribution of muons appears multi-peak. The average deposited energy of pions is less than that of muons because of the larger hit number.

(4) Second-moment  $S$ 

The second-moment<sup>[7]</sup>  $S$  is defined as  $S = \frac{\sum_i E_i \cdot d_i^2}{\sum_i E_i}$ , where  $E_i$  is the energy deposited in the  $i$ -th crystal, and  $d_i$  is the distance between the  $i$ -th crystal and the maximum energy deposited crystal in the reconstructed cluster. The original idea of  $S$  was developed by the Crystal Ball experiment to distinguish the cluster generated by  $\pi^0$  and  $\gamma$ .

A fraction of pions will have nuclear interaction

with the crystals, the energy distribution of pions is wider than muons, so that part of the second-momentum of pions is bigger.

(5) Energy deposited along the extrapolated path<sup>[8]</sup>

Energy deposited in a  $3 \times 4$  crystal matrix along the extrapolated path was summed up. Along the particle track direction the deposited energy distribution is wider, so a  $3 \times 4$  crystal matrix was used.

Comparing this variable with variable (1) i.e. the total energy deposited in the calorimeter, we can see that most of the energy deposited by muons was included in the matrix, but only a part of the energy deposited by pions was included in the matrix.

## (6) Number of crystals along the extrapolated path

All hit crystals in a  $3 \times 4$  matrix along the extrapolated path were counted.

The distribution of the number of crystals along the extrapolated path of muons is narrower than that of pions.

## (7) Number of hit crystals outside of the extrapolated path

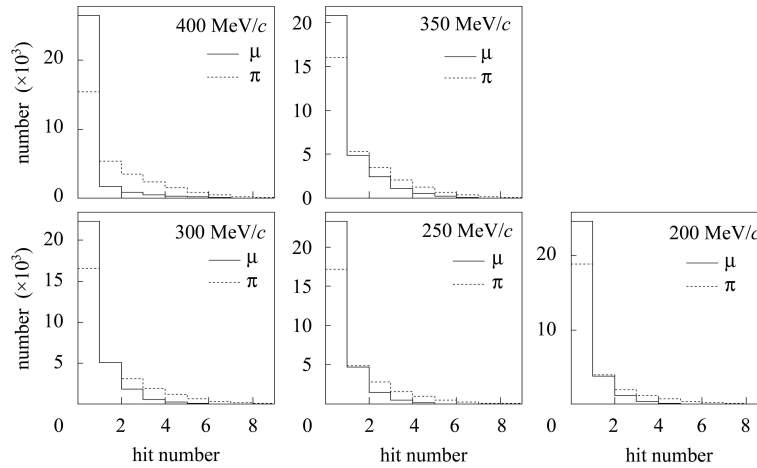


Fig. 10. Number of crystals beyond the extrapolated path for different momenta. Solid line stands for muons and dashed line stands for pions.

Crystals outside of the  $3 \times 4$  matrix along the extrapolated path but included in the reconstructed cluster were counted.

The number of crystals outside of the extrapolated path of muons is lower than that of pions.

## 5 Brief description of the artificial neural network

An artificial neural network<sup>[9]</sup> is a computational structure inspired by the study of biological neu-

ral processing. Feed-forward neural networks, also known as multilayered perceptrons, are most popular and widely used. A typical network is made of neurons characterized by a bias and weighted links in between, those links are called synapses. It is composed of an input layer, an output layer and sometimes one or more hidden layers. There is a weight for each connection between two neurons. The weights are established by a training procedure. The Multilayer Perceptrons<sup>[9]</sup> (MLP) network is trained in a supervised manner, generally with an algorithm known as back propagation of error. A layer of neurons makes

independent computations on the data, so that it receives and passes the results to another layer. The next layer may in turn make its independent computations and pass on the results to yet another layer. The output is calculated by weighting the sum of all the inputs weighted by corresponding elements of the weight matrix, and the output is then processed with a transfer function such as a linear or sigmoid function.

## 6 Preliminary result

In this paper, a class of Multilayer Perceptrons<sup>[10]</sup> (MLP) network with two hidden layers was applied to do the  $\mu$ - $\pi$  identification, which is implemented in ROOT<sup>[11]</sup>, since a neural network with two hidden layers is more efficient than that with one. The number of neurons varied with the number of input variables, following the rule of thumb that the number of hidden neurons should be about twice that of the input variables. Monte Carlo data were divided into two equal subsamples serving as the NN training sample and test sample.

Seven input variables described so far were used and the output of the neural network is illustrated in Fig. 11. Events with different  $\theta$  were studied. It can be seen that the study of  $\mu$ - $\pi$  separation yields a pion contamination rate of about 15% while keeping the muon identification efficiency at about 80% when the polar angle is  $90^\circ$ . The pion contamination rate will show deterioration when the polar angle became smaller while keeping the same muon identification

efficiency.

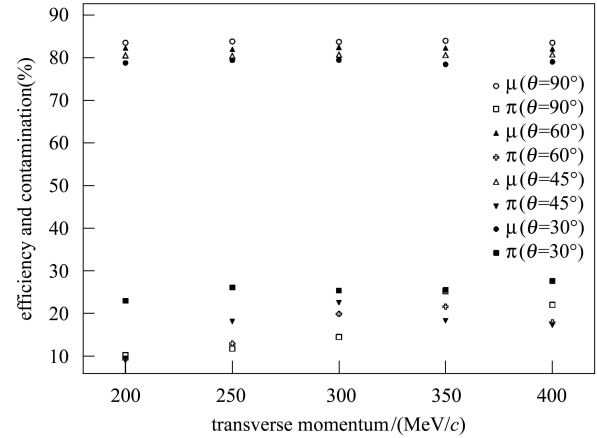


Fig. 11. The output of neural network.

## 7 Conclusion

Low momentum  $\mu$ - $\pi$  identification was studied in this paper, several useful discriminating variables were defined, and the result was satisfactory. The study of  $\mu$ - $\pi$  separation performed with momenta from 200 MeV/c to 400 MeV/c yielded a contamination rate from pions of about 15% with a neural network, while maintaining about 80% muon identification efficiency when the polar angle is  $90^\circ$ . When the polar angle became smaller the contamination rate will deteriorate. This will be a complementary method to the BESIII PID algorithm. The analysis strategy discussed in this paper can be applied to the BESIII PID algorithm with simple modification of the BESIII reconstruction package.

## References

- BESIII Design Report. Interior Document in Institute of High Energy Physics, 2004
- QIN Gang et al. Chinese Physics C (HEP & NP), 2008, **32**(1): 1—8
- LI Jia-Cai et al. HEP&NP, 2004, **28**(12): 1269—1277 (in Chinese)
- DENG Zi-Yan et al. HEP&NP, 2006, **30**(5): 371—377 (in Chinese)
- LI Wei-Dong, LIU Huai-Min et al. The Offline Software for the BESIII Experiment. Proceeding of CHEP06. Mumbai, India, 2006
- HE Miao. Simulation and Reconstruction for BESIII Electro-Magnetic Calorimeter, 2008
- Antreasyan D. An algorithm for tagging photon and merged  $\pi^0$  showers in the crystal ball. Crystal Ball note 321, 1983
- WANG Liang-Liang et al. HEP&NP, 2007, **31**(2): 183—188 (in Chinese)
- Valluru B. Rao. C++ Neural Networks and Fuzzy Logic. 1995
- Brun R, Rademakers F et al. ROOT Users Guid 5.12. 2006, 73—76
- Brun R, Rademakers F et al. An Object-Oriented Data Analysis Framework. <http://root.cern.ch>